Physicochem. Probl. Miner. Process., 62(5), 2026, 235676

http://www.journalssystem.com/ppmp

Physicochemical Problems of Mineral Processing

ISSN 1643-1049

Contribution of roughness parameter on coagulation and flocculation characteristics of fine chromite

Onur Güven [1], Yunus Emre Çavdar [2], Orhan Ozdemir [2]

[1] Adana Alparslan Türkeş Science and Technology University, Engineering Faculty, Mining Engineering Department, 01250, Sarıçam, Adana, Türkiye

[2] Istanbul Technical University, Mines Faculty, Mineral Processing Engineering Department, 34475, Maslak, Istanbul, Türkiye

Corresponding author: oguven@atu.edu.tr (Onur Güven)

Abstract: In this study, the coagulation and flocculation behavior of fine chromite particles was investigated as a function of surface roughness produced by the grinding process under different conditions. The specific contribution of surface roughness was evaluated using both experimental and theoretical approaches. In the experimental section, after the samples were ground in ball and rod mills, the particle size distribution was measured with a Malvern particle size analyzer, and surface roughness was characterized by optical profilometry and atomic force microscopy (AFM). Following physical characterization, coagulation tests were conducted using settling experiments with NaCl and $CaCl_2$ as coagulants. Subsequently, the flocculation performance was evaluated using the same experimental procedure with anionic (ENFLOC 5250AV, ECS Chemistry Co., Istanbul, Türkiye) and cationic flocculants (ENFLOC 425CA, ECS Chemistry Co., Istanbul, Türkiye). In addition to the experimental studies, theoretical analyses were conducted to support the experimental findings by calculating energy barrier heights. In conclusion, results from samples with varying surface roughness show that increasing surface roughness significantly affects the coagulation and flocculation behavior of fine chromite particles, a critical factor for subsequent processing.

Keywords: chromite, roughness, coagulation, flocculation, AFM

1. Introduction

Coagulation and flocculation are important processes, particularly in mineral processing, used to aggregate fine particles through particle-particle interactions (Ozun and Ulus, 2019; Guven et al., 2026). During these processes, various parameters, including the valence of coagulants, the type of flocculants (anionic or cationic), the concentrations of these reagents, the pH of the medium, and other physicochemical properties, influence the formation of bridges between fine particles (Ersoy, 2005). In addition to the properties of the reagents, the efficiency of these processes also depends on the physical properties of the particles, such as particle size, shape, density differences, and surface charge, all of which affect particle-particle interactions (Suresh et al., 1996; Guven et al., 2022; Guven et al., 2026).

As mentioned above, numerous studies have investigated parameters affecting coagulation and flocculation, including coagulant and flocculant types and concentrations, as well as medium pH (Ozkan, 2003; Amuda et al., 2007; Önen et al., 2018). However, compared to the extensive number of studies examining the role of particle morphology in flotation, studies investigating its effect on coagulation and flocculation are relatively few (Ulusoy et al., 2003; Yekeler et al., 2004; Verelli et al., 2014; Guven et al., 2015; Guven et al., 2020; Guven et al., 2022). For example, a recent review study highlighted the importance of particle morphology, alongside particle size, in mineral processing, mining, construction, and other engineering fields. The review concluded that understanding particle morphology enables optimization of reagent type and dosage, ultimately improving process efficiency (Ulusoy, 2023).

In another study, Zhang et al. (2024) investigated how Haynes 230 powder roughness affects fluidity. They concluded that as surface roughness increases, particles' surface energy also increases, reducing

DOI: 10.37190/ppmp/235676

flowability and, consequently, strengthening interparticle interactions. Furthermore, recent studies have investigated particle-particle interactions by evaluating particle coagulation and flocculation efficiencies (Gungoren et al., 2020) and correlating these results with zeta potential measurements under the same conditions (Megersa et al., 2019). These studies show that particle surface charge can indicate particle-particle interactions within a suspension (Suresh et al., 1996). From this perspective, theoretical calculations, together with experimental studies, can help determine optimal reagent concentrations and support experimental findings.

Therefore, a systematic investigation is needed to clarify how particle morphology, particularly surface roughness, affects particle coagulation and flocculation behavior. To the best of our knowledge, few studies have investigated the effect of particle morphology on the efficiency of coagulation and flocculation processes (Muhle, 1985; Shulepov, 1996; Guven et al., 2025; Guven et al., 2026). Given this information gap, the present study aimed to investigate the effect of particle roughness on the coagulation and flocculation of fine chromite particles using both experimental and theoretical approaches.

2. Materials and methods

2.1. Materials

The chromite samples used in this study were obtained from the Etibank Elazığ Ferrochrome Plant in Türkiye. The particle size distribution (PSD) of the samples was determined using a Retsch AS200 automatic sieve shaker. The PSD analysis of the sample showed that the d_{50} and d_{80} values were approximately 110 µm and 210 µm, respectively. The mineralogical structure and chemical composition of the sample were determined by X-ray diffraction (XRD) using a Rigaku MiniFlex instrument and X-ray fluorescence (XRF) using a Rigaku XRF instrument. During the XRD analysis, Cu Kα radiation generated by a long, finely focused Cu tube operating at 40 kV and 15 mA was used. The diffraction data were collected over a 2θ range of 5–90° at a scan rate of 2°/min. The XRD (Fig. 1) and XRF (Table 1) results showed that the sample consists predominantly of chromite and contains only trace impurities.

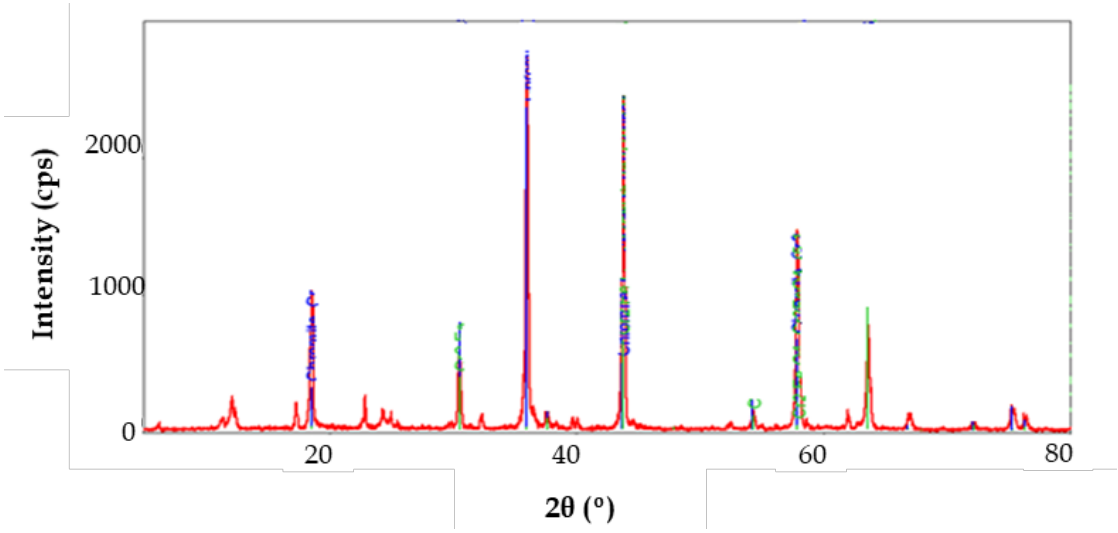

Fig. 1. XRD patterns for chromite sample

Table 1. X-ray fluorescence (XRF) analysis results of chromite sample

Cr_2O_3	Fe_2O_3	SiO_2	Al_2O_3	MnO	CaO	TiO_2	Other
54.57	26.50	8.20	8.00	1.17	0.51	0.24	0.81

Coagulation experiments were carried out using sodium chloride (NaCl) and calcium chloride ($CaCl_2$). Both chemicals were obtained from Tekkim Chem. (Bursa, Türkiye) in extra-pure quality. Flocculation experiments were conducted using commercial anionic (ENFLOC 5250AV, ECS Chemistry Co., Istanbul, Türkiye) and cationic (ENFLOC 425CA, ECS Chemistry Co., Istanbul, Türkiye) flocculants supplied by ECS Chemistry Co., Istanbul, Türkiye.

2.2. Methods

2.2.1. Grinding

Prior to the coagulation and flocculation experiments, grinding tests were conducted under various conditions to investigate the effects of particle size and surface roughness on particle coagulation and flocculation behavior. The grinding tests were performed using both ball and rod mills, following the experimental procedure described in our previous study (Guven et al., 2026). Laboratory-scale ball and rod mills were used during these tests. Steel balls with diameters of 30, 25, and 20 mm and steel rods with diameters of 31.7, 24.6, 15.9, and 9.8 mm were used as the grinding media. The volume of the ball mill was 5224 cm³ (diameter = 19.5 cm, length = 17.5 cm), whereas the volume of the rod mill was 7850 cm³ (diameter = 20 cm, length = 25 cm). Fig. 2 shows representative photographs of the grinding units.

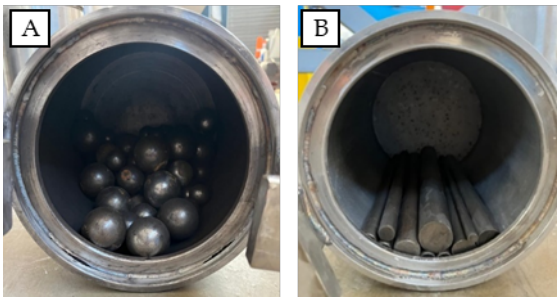

Fig. 2. (A) Representative photographs of the ball mill and (B) rod mill

The samples were ground in the mills for 20-25 min. After grinding, wet sieving was performed to ensure the entire sample had a particle size of less than 38 µm. Subsequently, the particle size distribution of the ground samples (< 38 µm) was determined using a Mastersizer 3000 laser particle size analyzer (Malvern Instruments Ltd., Malvern, UK) equipped with a wet dispersion unit. All measurements were performed at a stirring speed of 2000 rpm and an obscuration level of approximately 7 wt.% (by weight). Fig. 3 shows the particle-size distribution results for the ground samples.

As shown in Fig. 3, the particle-size distributions of the samples ground under different grinding conditions are very similar. The average d_{80} values were 40 µm for the sample ground in the ball mill and 32 µm for the sample ground in the rod mill. Therefore, as stated above, the effect of particle size distribution on the coagulation and flocculation experiments was minimized. The ground samples were subsequently characterized for surface roughness and then used in the coagulation and flocculation tests.

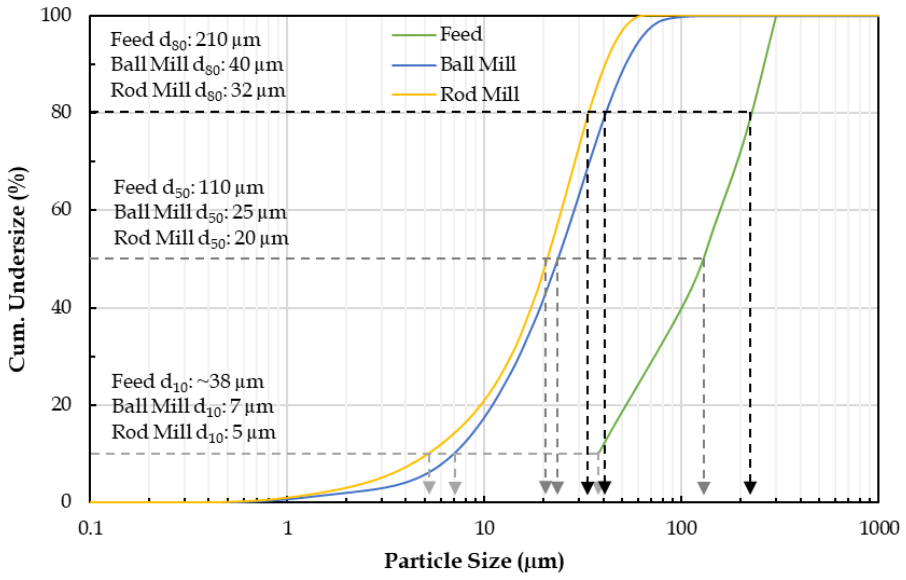

Fig. 3. Particle size distribution of chromite feed (wet sieve analysis) and ball and rod mill products (Malvern Mastersizer 3000)

2.2.2. Particle roughness analysis

After the grinding, the surface roughness of fine chromite particles produced under different grinding conditions was characterized using two techniques: Atomic force microscopy (AFM) and optical profilometry. AFM analysis was performed using an NX100 model Atomic Force Microscope (Park Systems) operated in "tapping" mode with a 5 × 5 μm² scan area. Representative AFM images are shown in Fig. 4.

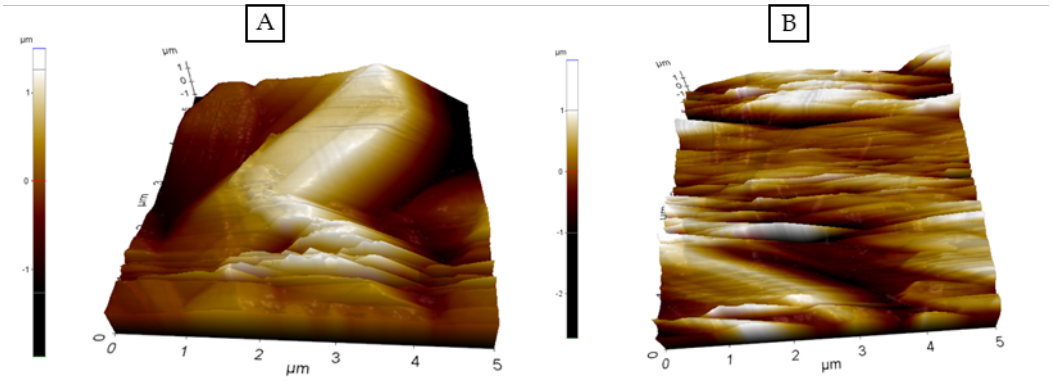

Fig. 4. (a) AFM picture of ground chromite (a) Ball mill (Ra: 437 nm) (b) rod mill (Ra: 165 nm)

A contact-type cantilever was used for the AFM measurements. Although various surface roughness parameters, such as skewness (*Rsk*) and kurtosis (*Rku*), can be obtained using this instrument, only the average surface roughness (*Ra*) was used to evaluate the effects of different grinding media. The literature has proposed various approaches for characterizing surface roughness. For example, assumptions based on Gaussian height distributions (Tayebi et al., 2004) and the Greenwood-Williamson model have been widely used to characterize engineering surfaces. However, in mineral processing, the average surface roughness (*Ra*) is generally considered sufficient to evaluate the contribution of surface roughness to particle-particle and bubble-particle interactions (Guven et al., 2022; Guven et al., 2026). In addition to AFM measurements, the surface roughness of the samples was characterized using an optical profilometer (Filmmetrics Profilm3D), which enables measurements over a larger surface area. Fig. 5 shows representative optical profilometer images of the samples.

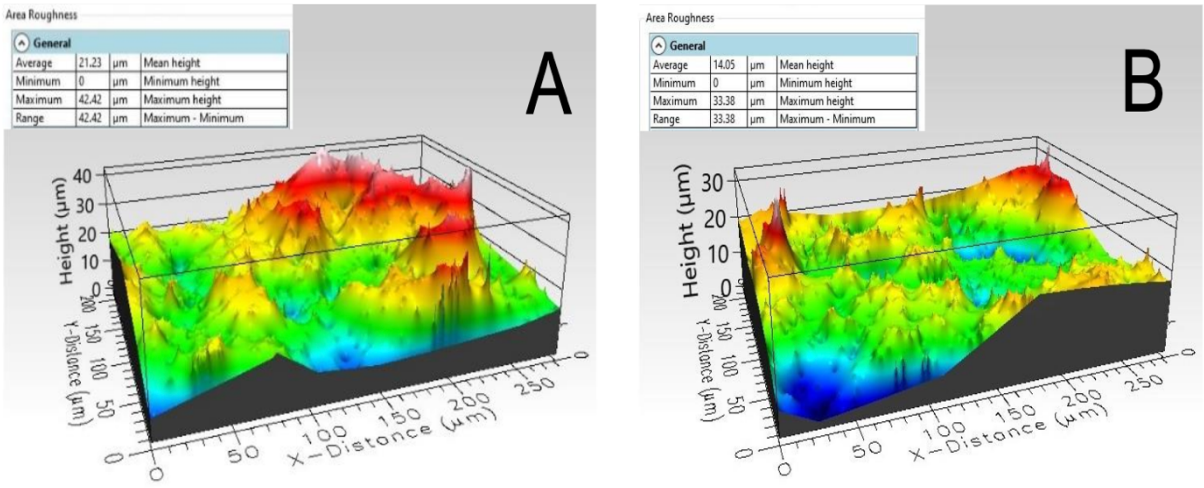

Fig. 5. The optical profilometer pictures of chromite (A: Ball mill) (B: Rod mill)

In addition to AFM and optical profilometry, the Brunauer–Emmett–Teller (BET) method can estimate surface properties via specific surface area measurements from nitrogen adsorption (Rezai et al., 2010; Guven et al., 2015). However, AFM and optical profilometry provide a more direct and representative characterization of particle surface roughness.

Table 2. Roughness results of samples used in the experimental studies measured using an optical profilometer and AFM

	Ball Mill	Rod Mill
Profilometer	21.23 μm	14.05 μm
Atomic Force Microscopy	437 nm	165 nm

As shown in Table 2, although the average surface roughness values obtained from different devices are reported in different units and measured over different surface areas, the general trends remain consistent despite the structural differences in the effective measurement areas of each technique. A similar relationship was also reported in a previous study (Mei and Guan, 2023). In the study, roughness values obtained via AFM were more accurate than those from optical profilometry, indicating that a smaller sampling area can provide more representative information about particle morphology. These results allow broader evaluation of the effects of particle surface roughness on coagulation and flocculation in subsequent analyses.

2.2.3. Coagulation and flocculation experiments

In this study, two different methods were used to measure particle coagulation and flocculation: settling rate tests and turbidity measurements:

(I): Settling rate tests: Similar to the experimental setup reported in our previous study (Celik et al., 2024). The tests were conducted in a standard cylindrical glass measuring cell (78.7 × 78.7 × 317.5 mm) with a working volume of 250 cm^3. In all experiments, suspensions with a solid concentration of 3% (by weight) and a total volume of 250 cm^3 were prepared using distilled water with a conductivity of 20 μS/cm. Coagulant and flocculant additions were performed at the natural pH (approximately 8.0) of the chromite suspensions. The suspensions were stirred in a graduated cylinder at 360 rpm for 5 min using an appropriately sized magnetic stirrer, and time-dependent settling behavior was then recorded. Measurements were taken every 10 sec. Average values were used to generate height-versus-time curves. During the experiments, the height of the clarified zone was recorded at each time point, and the settling rate (cm/sec) was calculated from the slope of the resulting curves. Although a linear settling trend is generally expected for solid concentrations below 5% (by weight), the types of coagulant and flocculant used, as well as particle surface roughness, can cause deviations from this behavior.

(II): Turbidity measurements: The turbidity of the suspensions was determined using a portable turbidimeter (Lovibond Turbidirect model) in accordance with DIN ISO 27027, which is equivalent to TS EN ISO 7027-1. The details of the method were reported in our previous study (Celik et al., 2024). Turbidity measurements were performed by transferring 12 cm^3 of suspension into glass cuvettes specifically designed for the turbidimeter. The suspensions were prepared at various coagulant and flocculant concentrations, with a solid concentration of 3% (by weight), to mimic the conditions used in the settling rate tests closely. Prior to measurement, the samples were conditioned for 5 min at 420 rpm using a 20 × 5 mm magnetic stir bar, in accordance with the settling tests. Turbidity values (NTU, nephelometric turbidity units) were recorded at 15, 30, 45, and 60 sec.

2.2.4. Zeta potential measurements

Zeta potential measurements were performed using a microelectrophoresis method with a microprocessor-equipped Zeta Plus instrument (Brookhaven Instruments, NY, USA). The instrument automatically calculates zeta potential values based on the applied voltage and the particles' electrophoretic velocity. The sample chamber is made of Plexiglas. During the measurements, the applied voltage was adjusted based on the suspension's conductivity. Due to excessively high conductivity, zeta potential measurements could not be performed at pH values below 2.5 or above 11.5. During the measurements, particle motion was monitored on the instrument screen while the electrodes were connected to the anode and cathode terminals, as indicated by their color coding. An average of 10 measurements was performed for each sample prepared at a solid concentration of 1% (by weight) in the pulp. The instrument automatically calculated the zeta potential values, and the mean and standard deviation were recorded.

2.2.5. Energy barrier analysis

The extended Derjaguin–Landau–Verwey–Overbeek (XDLVO) theoretical approach, which has several variants in the literature (Suresh et al., 1996; Guven et al., 2015; Guven et al., 2021), was used to calculate the energy barrier between particles. In these calculations, particle surfaces are generally assumed to be smooth, and the dominant parameters are the zeta potential and the Debye length, which are measured under various conditions. However, incorporating surface roughness values into the model can yield more representative correlations with experimental results. This is because no material surface is perfectly smooth, and even minor roughness variations can significantly influence particle–particle interactions (Drelich and Bowen, 2016).

Furthermore, in this study, the Debye length varies alongside the zeta potential during coagulation and flocculation experiments conducted with salt solutions. Consequently, the impact of these variations on theoretical predictions can also be evaluated. The equations used in the calculations are presented below:

For smooth particles;

$$E_{vdw-SPS} = 2\pi RA\left[\frac{-2.45\lambda}{120\pi^2h^2} + \frac{2.17\lambda^2}{720\pi^3h^3} - \frac{0.59\lambda^3}{3360\pi^4h^4}\right] \text{ (vdW)} \quad (1)$$

$$E_{EDL-SPS} = 16R(4\pi\varepsilon\varepsilon_0)(\frac{kT}{e})^2 tanh(\frac{e\varphi_1}{4kT})tanh(\frac{e\varphi_2}{4kT})e^{-\kappa h} \text{ (EDL)} \quad (2)$$

$$E_{H-SS} = -2\gamma_{hw}H_y e^{-h/D_H} \text{ (Hydrophobic)} \quad (3)$$

For rough particles;

$$E_{vdW-RPS} = 2\pi RA\left[\frac{-2.45\lambda}{120\pi^2h^2} + \frac{2.17\lambda^2}{720\pi^3h^3} - \frac{0.59\lambda^3}{3360\pi^4h^4}\right] + n\pi\left(\frac{2.45\lambda AR}{30\pi}\right)\left[\frac{{\epsilon_s}^2}{2h^2} + ln\left(\frac{h}{h-\epsilon_s}\right) - \frac{\epsilon_s}{h-\epsilon_s}\right] -$$
$$n\pi\left(\frac{2.17\lambda^2 AR}{360\pi^2}\right)x\left[{\epsilon_s}^2\left(\frac{1}{h^3} - \frac{1}{(h-\epsilon_s)^3}\right) - \frac{1}{h} + \frac{1}{h-\epsilon_s} - \frac{\epsilon_s}{(h-\epsilon_s)^2} + \frac{{\epsilon_s}^2}{(h-\epsilon_s)^3}\right] + n\pi\left(\frac{0.59\lambda^3 AR}{840\pi^3}\right)$$
$$x\left[{\epsilon_s}^2\left(\frac{1}{2h^4} - \frac{1}{2(h-\epsilon_s)^4}\right) - \frac{1}{6h^2} + \frac{1}{6(h-\epsilon_s)^2} - \frac{\epsilon_s}{3(h-\epsilon_s)^3} + \frac{{\epsilon_s}^2}{2(h-\epsilon_s)^4}\right] \text{ (vDW)} \quad (4)$$

$$E_{EDL-RPS} = 16R(4\pi\varepsilon\varepsilon_0)\left(\frac{kT}{e}\right)^2 tanh\left(\frac{e\varphi_1}{4kT}\right)tanh\left(\frac{e\varphi_2}{4kT}\right)(1 - n\pi{\epsilon_s}^2)e^{-kh}$$
$$+\frac{8n\pi\epsilon_s}{\kappa}R(4\pi\varepsilon\varepsilon_0)\left(\frac{kT}{e}\right)^2 tanh\left(\frac{e\varphi_1}{4kT}\right)\gamma_3 e^{-\kappa(h-\epsilon_s)} \text{ EDL)} \quad (5)$$

$$E_{H-SS} = -4\pi R\gamma_{hw}H_y D_H(1-\theta)\exp\left(\frac{-h}{D_H}\right) - 8\pi Rn\gamma_{hw}H_y\epsilon_s{D_H}^2 exp\left(\frac{-h+\epsilon_s}{D_H}\right) \text{ (Hydrophobic)} \quad (6)$$

These equations include several parameters, which are defined as follows: A is the Hamaker constant (J); D is the particle diameter (m); D_H is the characteristic distance used in the calculation of hydrophobic interactions (m); e is the elementary charge (C); h is the separation distance (m); H_y is the hydrophobicity parameter; k is the Boltzmann constant (J K^{-1}); n is the roughness density (m^{-2}, defined as $\theta/\pi\varepsilon_s^2$); R is the radius of a spherical particle (m); T is the temperature (K); Y_3 is the effective surface charge of rough surfaces (V); ε is the dielectric constant of the bulk medium; ε_0 is the permittivity of free space (C^2 J^{-1} m^{-1}); ε_s is the roughness radius (m); $\gamma_{HW}$is the hydrophobic surface–water interfacial tension (J m^{-2}); κ^{-1} is the Debye length (m); λ is the characteristic wavelength for van der Waals interactions (m); ψ_1, ψ_2, and $\psi_3$are the surface potentials of the particle and roughness elements (V); and θ represents the surface roughness level.

Most of these parameters are constant; in contrast, the particle–particle energy barrier is primarily determined by variations in particle diameter, Hamaker constant, zeta potential, Debye length, and surface roughness.

3. Results and discussion

3.1. Coagulation and flocculation experiments

3.1.1. Settling rate tests

As stated in the introduction, settling rate tests were conducted using chromite samples with varying surface roughness values in the presence of NaCl and $CaCl_2$ at various concentrations. During these

tests, the settling rate of chromite in pure water averaged 0.1150 cm/sec. This value increased slightly with increasing NaCl concentration, reaching 0.1161 cm/sec. In experiments with $CaCl_2$, the settling rate increased further to 0.1172 cm/sec as salt concentration increased. Table 3 and Fig. 6 show the results.

Table 3. Settling rate of chromite samples in NaCl and $CaCl_2$ solutions

	Concentration (mol/dm³)	Ball Mill Product (cm/sec)	Rod Mill Product (cm/sec)
NaCl	$1x10^{-5}$	0.1131	0.1161
	$1x10^{-4}$	0.1157	0.1163
	$1x10^{-3}$	0.1160	0.1164
	$1x10^{-2}$	0.1166	0.1144
	$1x10^{-1}$	0.1161	0.1134
$CaCl_2$	$1x10^{-5}$	0.1131	0.1161
	$1x10^{-4}$	0.1136	0.1172
	$1x10^{-3}$	0.1166	0.1150
	$1x10^{-2}$	0.1137	0.1127
	$1x10^{-1}$	0.1118	0.1116

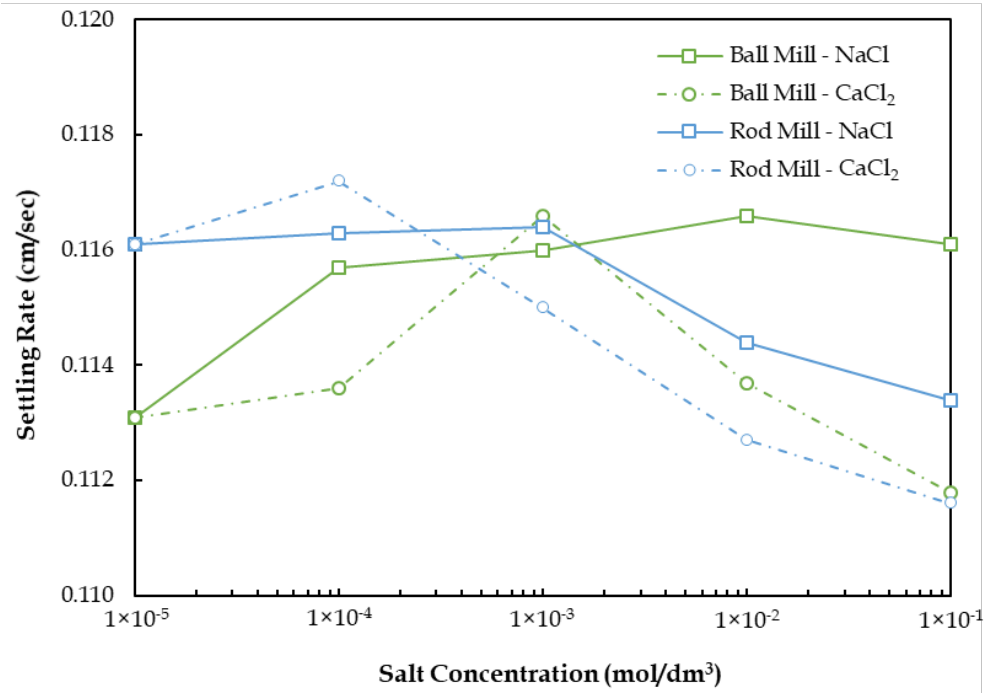

Fig. 6. Coagulation results of chromite particles as a function of NaCl and $CaCl_2$ concentrations

As shown in Fig. 6, the effect of particle surface roughness was evaluated at a constant NaCl concentration of 1×10^{-3} mol/dm³. The settling velocities of particles with a roughness of 21.23 µm, obtained via ball milling, were determined to be 0.1160 cm/sec and 0.1166 cm/sec in NaCl and $CaCl_2$ solutions, respectively. In contrast, for particles obtained by rod milling under the same conditions and having a roughness of 14.05 µm, the corresponding settling velocities were 0.1164 cm/sec and 0.1150 cm/sec.

In a previous study we conducted on chromite coagulation, a lower settling rate of 0.0857 cm/sec was reported for particles ground in a ball mill (an average roughness of 1.920 µm *Ra*) in 1×10^{-3} mol/dm³ NaCl. In contrast, a higher value of 0.0917 cm/sec was observed for particles ground in a rod mill (2.581 µm *Ra* value) (Guven et al., 2026). Based on these results, surface roughness appears to affect particle–particle interaction rates up to a certain threshold; this behavior will be discussed in greater detail in the theoretical section.

Furthermore, the difference between the present and previous studies can also be attributed to the higher fraction of fine particles in the previous study, another factor influencing coagulation behavior. Overall, these findings highlight the importance of considering particle surface roughness, in addition to salt type and concentration, for a more comprehensive understanding of coagulation and flocculation processes in fine particle systems.

3.1.2. Flocculation experiments

In this study, the effects of different concentrations (5, 10, and 15 g/Mg) of anionic and cationic flocculants on the flocculation behavior of particles with different surface roughness values were evaluated in terms of settling rate, similar to the coagulation tests. The results are shown in Table 4 and Fig 7.

Table 4. Settling rates of chromite samples in the presence of anionic and cationic flocculants at different concentrations

	Concentration (g/Mg)	Ball Mill Product (cm/sec)	Rod Mill Product (cm/sec)
Anionic	5	0.9736	1.0736
	10	1.0771	1.0208
	15	1.3992	0.9504
Cationic	5	0.7725	0.9565
	10	1.056	1.0736
	15	1.364	1.3816

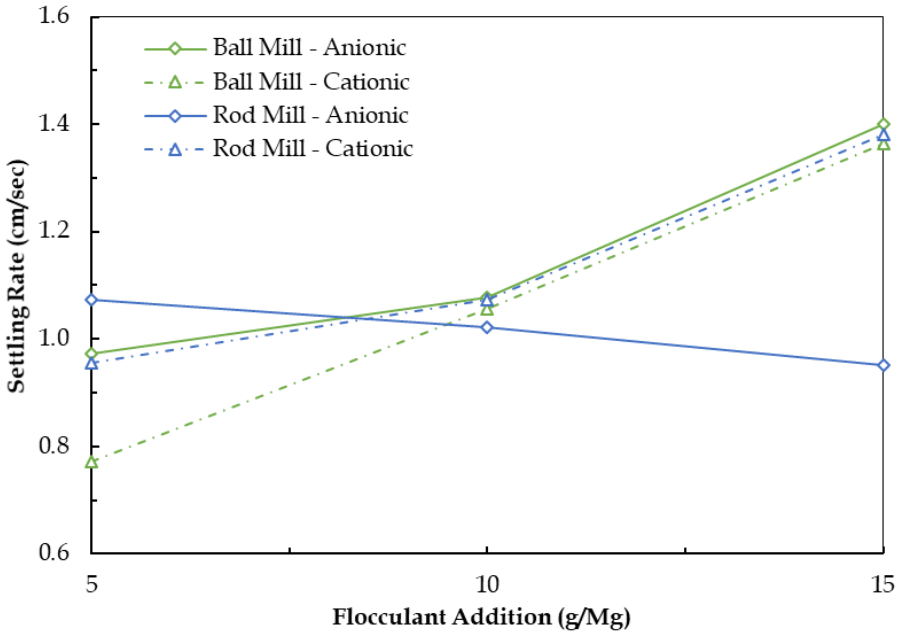

Fig. 7. Flocculation results of chromite particles as a function of flocculant dosage (g/Mg)

The effect of flocculant addition on the settling rate of chromite particles ground under different grinding conditions is shown in Fig. 7. As shown in Fig. 7, the settling rate increased in most systems when the flocculant dosage increased from 5 to 15 g/Mg; this indicated improved floc formation, which promoted greater aggregation and settling. However, the magnitude of this response depends largely on both the flocculant type and the particles' grinding environment. In this way, using a cationic flocculant for samples ground in a ball mill resulted in a significant increase in the settling rate, with a peak value of approximately 1.4 cm/sec at a dosage of 15 g/Mg. This behavior suggests strong electrostatic attraction between the negatively charged chromite surfaces and the cationic polymer

chains, promoting effective polymer bridging and floc formation. In contrast, the anionic flocculant showed a weaker response for the same sample type. Thus, the sample ground in the rod mill showed a different trend. While the anionic flocculant performed better at higher dosages, the response to the cationic flocculant was less pronounced. This suggests that changes in surface properties (particularly surface morphology and roughness) from different grinding media affect polymer adsorption and flocculation efficiency. The differences between ball-milled and rod-milled particles further demonstrate that surface roughness and heterogeneity play a significant role in determining particle–polymer interactions. These findings indicate that particles ground in a ball mill are more sensitive to flocculant addition, likely because of increased surface area and more active sites conducive to polymer adsorption. The fact that the increase in settling rate at higher dosages does not follow a strictly linear trend may suggest the onset of saturation effects or partial re-stabilization due to excess polymer in the solution.

Overall, the results indicate that flocculant type, dosage, and particle surface properties determine flocculation performance. Particle morphology resulting from different grinding conditions significantly influences the efficiency of polymer-mediated aggregation and settling behavior.

3.2. Turbidity measurements

3.2.1. Coagulation experiments

In addition to settling rate tests, the effects of coagulants at various concentrations on the coagulation behavior of particles with different surface roughness values were evaluated in terms of turbidity. Fig. 8 presents the results.

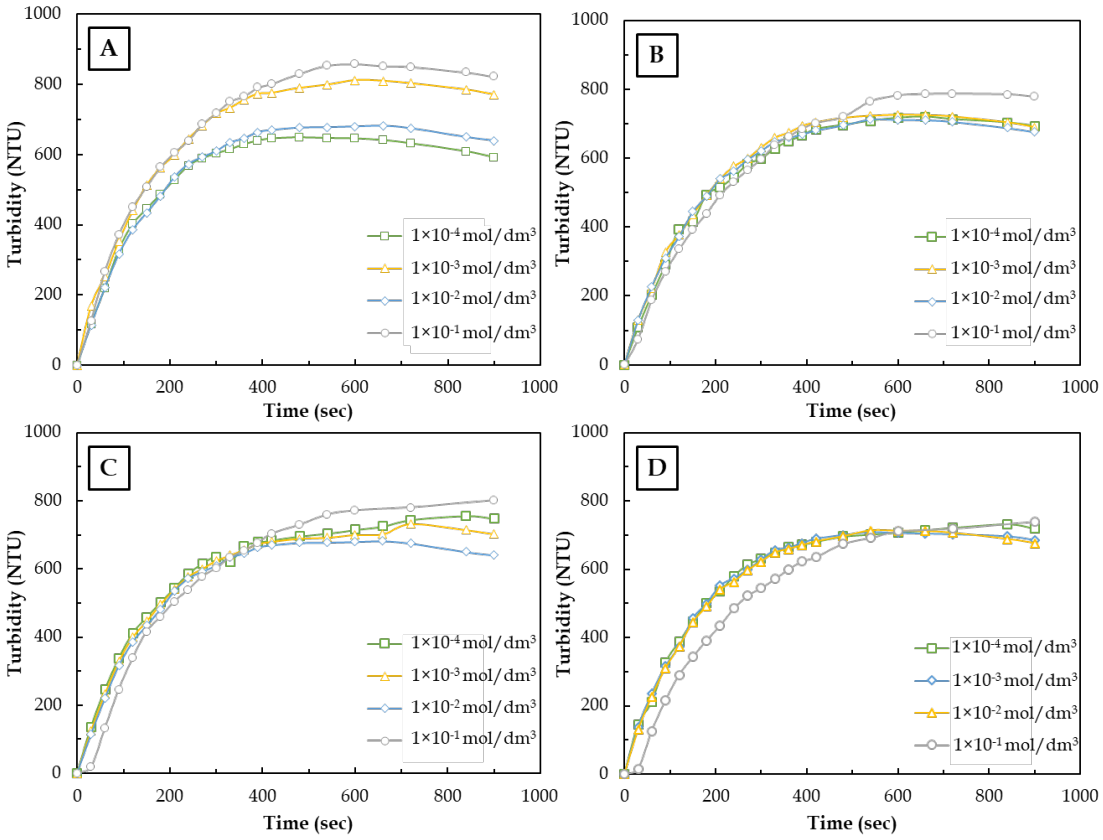

Fig. 8. Turbidity values obtained for NaCl (A-Ball Milled, B-Rod Milled) and $CaCl_2$ (C-Ball Milled, D-Rod Milled)

As stated in the introduction, the coagulation behavior of fine chromite particles was evaluated by combining settling rate measurements with time-dependent changes in turbidity under various electrolyte concentrations and grinding conditions. Accordingly, the settling tests demonstrated that the settling rate of chromite in pure water was 0.1150 cm/sec, and that this rate increased further with the addition of NaCl (0.1161 cm/sec at 1×10^{-3} mol/dm^3) and $CaCl_2$ (0.1172 cm/sec at the same

concentration). This gradual increase, consistent with classical DLVO theory, indicates that adding electrolytes promotes particle aggregation by compressing the electrical double layer and reducing repulsive interactions. In this context, the turbidity results (Fig. 8) provide a more detailed understanding of inter-particle interactions. In all cases, turbidity increased rapidly during the initial stages and approached a plateau after approximately 400–600 sec, reflecting gradual suspension stabilization before sedimentation. However, significant differences were observed, consistent with the settling rate tests, depending on both the milling method and the electrolyte concentration.

The samples prepared via ball milling exhibited higher final turbidity values than those prepared via rod milling; notably, at a higher ionic strength (1×10^{-1} mol/dm^3), the value reached approximately 850 NTU. This behavior indicates that ball milling generates more surface defects and greater roughness (21.23 μm) than rod milling (14.05 μm), thereby increasing the sensitivity of interparticle interactions to electrolyte concentration. When the turbidity results are evaluated alongside settling rate data, a consistent trend emerges. Systems exhibiting higher turbidity generally correspond to more pronounced aggregation behavior in settling tests. For instance, the slight increase in settling rate observed as NaCl and $CaCl_2$ concentration rise is consistent with the enhanced particle interactions inferred from changes in turbidity. The higher efficiency of $CaCl_2$ than NaCl in promoting settling can be attributed to divalent Ca^{2+} ions, which more effectively compress the electrical double layer and facilitate interparticle bridging, leading to more rapid aggregation. When both datasets are considered together, the influence of grinding conditions is also clear; particles ground in a ball mill, which showed higher turbidity responses and greater sensitivity to electrolyte concentration, also displayed more pronounced changes in settling behavior. This indicates that increased surface roughness and heterogeneity enhance the effect of ionic strength on interparticle interactions. In contrast, rod-milled particles showed more stable turbidity behavior and only minor variations in settling rate because their surfaces were relatively smoother and less sensitive to changes in solution chemistry. Overall, the results demonstrate that the coagulation–flocculation performance of chromite suspensions is governed by the interplay among electrolyte type, ionic strength, and grinding-induced particle surface characteristics. The consistency between turbidity evolution and settling rate measurements confirms that particle aggregation mechanisms are strongly influenced by both electrical double-layer compression and surface roughness, consistent with DLVO/XDLVO-based interpretations.

3.2.2. Flocculation experiments

The effects of anionic and cationic flocculants on the flocculation behavior of particles with varying surface roughness were also evaluated using turbidity measurements. Fig. 9 illustrates the variation in suspension turbidity with conditioning time for ball-mill and rod-mill products at collector dosages of 5, 10, and 15 g/Mg. The two experimental conditions showed markedly different turbidity responses, demonstrating that both the grinding environment and reagent dosage significantly influence the dispersion and aggregation behavior of fine particles.

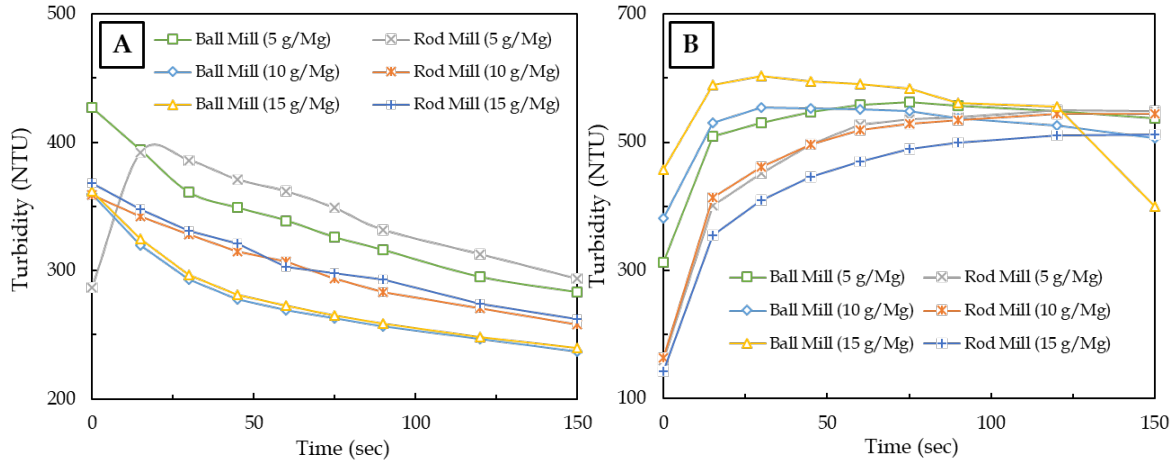

Fig. 9. Turbidity values obtained for anionic flocculant (A) and cationic flocculant (B)

In the first experimental condition (Fig. 9A), turbidity gradually decreased across all samples as conditioning time increased, indicating that suspended particles were progressively removed through aggregation and subsequent settling. The reduction was most pronounced during the first 60–90 sec; thereafter, the rate of turbidity decrease slowed significantly. This indicates that most coarse and medium-sized aggregates had already settled, while finer particles remained in suspension. Among the conditions tested, the ball mill product conditioned with 15 g/Mg reagent exhibited the lowest residual turbidity throughout the experiment, decreasing from approximately 325 NTU to around 235 NTU after 150 sec. This behavior demonstrates superior particle aggregation and more efficient settling compared with the other samples. In contrast, the ball mill product treated with 10 g/Mg consistently exhibited the highest turbidity values, remaining around 390 NTU at the start of the test and approximately 290 NTU after 150 sec, indicating poorer aggregation and slower settling. Meanwhile, the rod mill products displayed intermediate behavior, with turbidity steadily decreasing throughout the conditioning period. These observations suggest that both the grinding mode and the reagent dosage influence particle surface properties, thereby affecting interparticle interactions and settling kinetics.

Fig. 9B shows a distinctly different trend: instead of decreasing, turbidity increased rapidly during the initial conditioning stage and then stabilized at approximately 500–600 NTU for most treatments. This rapid increase within the first 20–40 sec indicates that continuing the conditioning process promoted the liberation and suspension of ultrafine particles, resulting in a higher concentration of dispersed solids within the pulp. After approximately 60–80 sec, only minor changes were observed, indicating the establishment of a dynamic equilibrium between particle dispersion and aggregation. The ball mill products, particularly at the highest dosage (15 g/Mg), generally exhibited higher equilibrium turbidity compared to the rod mill products. This observation is consistent with the tendency of ball milling, due to impact-dominated breakage mechanisms, to generate a higher proportion of ultrafine particles; in contrast, the rod milling process, characterized primarily by line-contact abrasion, typically produces a narrower particle size distribution with less generation of fines. The increasing concentration of ultrafine particles generated during ball milling can enhance suspension stability through mechanisms such as intensified Brownian motion, electrostatic repulsion, and hydration forces, thereby reducing settling rates and maintaining higher turbidity levels. The contrasting behavior observed between Figs. 9a and 9b highlights the dual role of reagent dosage in mineral processing systems. Under certain conditions, increasing reagent dosage promoted particle aggregation and accelerated sedimentation, resulting in lower turbidity. However, under the second set of experimental conditions, increasing the dosage did not improve clarification; instead, turbidity remained high, suggesting that excessive reagent adsorption may have re-stabilized particle surfaces or enhanced dispersion of ultrafine particles. Similar behavior has been reported in flotation and slurry conditioning studies, where reagent overdose or excessive slime production can inhibit flocculation by increasing electrostatic or steric repulsive forces between particles. From a mineral processing perspective, these results demonstrate that the effectiveness of reagent addition largely depends on the particle-size distribution produced during grinding. While the low turbidity observed in rod mill products indicates improved settling characteristics and reduced slime dispersion, the high turbidity associated with ball mill products points to greater production of ultra-fines that can remain in suspension for extended periods. Because excessive fines adversely affect flotation through mechanisms such as slime coating, increased reagent consumption, and reduced selectivity, controlling grinding conditions is as important as optimizing reagent dosage.

Overall, the results indicate that the interaction between grinding method and reagent dosage determines suspension stability and particle aggregation. The ball mill product treated with 15 g/Mg reagent achieved the most effective clarification under settling conditions (Fig. 9A). In contrast, in the second condition (Fig. 9B), the same treatment produced one of the most stable suspensions, characterized by the highest turbidity values. These findings demonstrate that process optimization must consider both grinding strategy and reagent dosage to achieve the desired balance between particle liberation, suspension stability, and downstream separation efficiency.

3.3. Zeta potential measurements

Similarly, an examination of the changes in chromite zeta potential at a salt concentration of 1×10^{-3} mol/dm^3 (Fig. 10A) reveals that the zeta potential of the chromite particles increased from 0.72 mV to

4.83 mV upon the addition of NaCl, and then to +19.9 mV following the addition of $CaCl_2$. Although this shift might suggest particle dispersion, maintaining the medium pH at its natural value after salt addition prevented Ca^{2+} ions from playing an active role, indicating that differences in coagulation characteristics can be attributed to changes in the Debye length. For zeta potential measurements with different flocculants, increasing the anionic flocculant concentration (starting from 5 g/Mg dosage) shifted the value from -4.72 mV to -22.09 mV. In contrast, adding 5 g/Mg cationic flocculant changed the value from -4.69 mV to -25.36 mV.

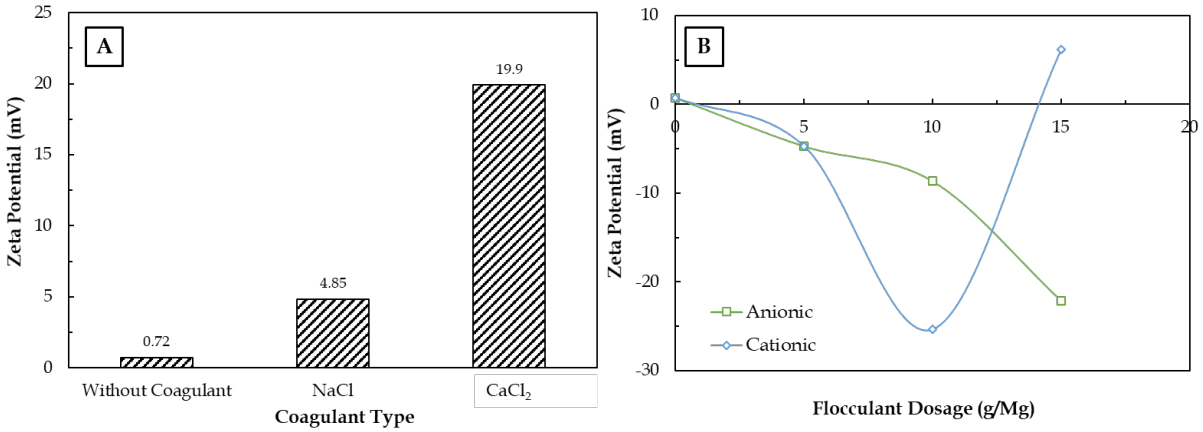

Fig. 10. Zeta potential results for chromite in the presence of (A) coagulants (1×10^{-3} mol/dm^3) and (B) flocculants at various dosages

The electrokinetic properties of the mineral suspension following coagulation and flocculation processes are presented in Fig. 10. The measured zeta potentials indicate that both the type of coagulant and the ionic character of the flocculant significantly affected the surface charge of the particles, and consequently, their aggregation behavior. In the absence of electrolyte, the suspension exhibited a zeta potential of 0.72 mV, revealing that the particles were near their isoelectric point. Under these conditions, electrostatic repulsive forces are minimized, and particle aggregation is expected to occur readily via van der Waals attractive forces.

While the addition of NaCl slightly increased the zeta potential to +4.85 mV, $CaCl_2$ resulted in a much higher positive value (+19.9 mV), indicating that Ca^{2+} ions adsorbed onto the negatively charged mineral surface, causing a partial charge reversal. The stronger effect of $CaCl_2$ is attributed to the higher valence of Ca^{2+}, which enhances electrical double-layer compression and promotes specific ion adsorption, both of which facilitate particle coagulation. After coagulation, adding polymer further altered the surface charge. In the case of the anionic flocculant, the zeta potential shifted from −4.72 mV at 5 g/Mg to −8.64 mV at 10 g/Mg, and subsequently decreased to −22.09 mV at 15 g/Mg. The relatively low absolute zeta potential values measured at 5 and 10 g/Mg indicate that the suspension remained electrokinetically unstable and prone to particle aggregation. In contrast, the significantly more negative value at 15 g/Mg indicates that excessive adsorption of anionic functional groups increased surface charge, allowing the suspension to become partially re-stabilized.

A similar trend was observed for the cationic flocculant. The zeta potential shifted from −4.69 mV at 5 g/Mg to −25.36 mV at 10 g/Mg, subsequently changing sign to +6.16 mV at 15 g/Mg. While the highly negative value at the intermediate dosage indicates surface overcharging, the positive value at the highest dosage shows that continued adsorption of cationic polymer chains first neutralized the charge, then reversed it. These observations reveal that the adsorption behavior of both polymers is dosage-dependent and that the addition of excessive amounts of reagent alters the electrokinetic conditions governing particle aggregation. The electrokinetic measurements are consistent with the turbidity variations presented in Figs. 6 and 7. Regardless of the electrolyte system, turbidity increased rapidly during the initial stage and approached a plateau after approximately 500–600 sec, indicating that the suspensions reached a quasi-equilibrium state. Although the overall kinetic profiles were similar, the equilibrium turbidity value depended on the electrolyte concentration.

In both electrolyte systems, suspensions prepared with 1×10^{-1} mol/dm^3 electrolyte exhibited the highest residual turbidity, whereas lower electrolyte concentrations generally resulted in lower equilibrium turbidity values. This behavior suggests that increasing ionic strength does not necessarily improve clarification. Although higher electrolyte concentrations effectively compress the electrical double layer, excessive ionic strength can increase residual turbidity by promoting the formation of smaller or more loosely structured aggregates that remain suspended longer.

The settling experiments (Figs. 6 and 7) further support this interpretation. For both the ball-mill and rod-mill products, turbidity decreased continuously with settling time, indicating progressive clarification of the suspensions. However, the extent of turbidity reduction depended on flocculant dosage. While the lowest residual turbidity values were generally achieved within the 5–10 g/Mg dosage range, only limited additional improvement, or, in some cases, slightly poorer clarification, was observed at 15 g/Mg. This trend is consistent with the zeta potential measurements. At moderate dosages, the absolute zeta potential remained below approximately +10 mV, indicating sufficient destabilization to promote polymer bridging and floc growth. Increasing the dosage beyond this level led to significant changes in surface charge: a decrease in zeta potential to −22.09 mV, particularly when using an anionic flocculant, indicating increased electrostatic stabilization due to excessive polymer adsorption.

This behavior is consistent with polymer overdosing, in which complete surface coverage limits floc formation by reducing the availability of free polymer segments for interparticle bridging. A comparison of the two grinding products also reveals differences in flocculation performance. Under comparable reagent conditions, the ball-mill product generally exhibited lower residual turbidity than the rod-mill product, indicating more efficient solid-liquid separation. This difference can be attributed to variations in particle size distribution and specific surface area resulting from the grinding method. The finer particles produced by ball milling provide a larger surface area for polymer adsorption, thereby enhancing bridge formation and promoting the development of larger, more compact flocs. Conversely, the relatively coarser rod-mill product may result in less effective polymer bridging due to differences in particle collision frequency and in the number of available adsorption sites.

The discrepancy between the zeta potential and settling rate trends indicates that electrostatic interactions were not the dominant mechanism controlling chromite flocculation. Although the zeta potential changed markedly with flocculant dosage, particularly for the cationic polymer, the settling behavior did not follow the same pattern. This suggests that polymer bridging, rather than charge neutralization, was the primary flocculation mechanism. In polymer-induced flocculation, large flocs can form while particles retain a significant surface charge because long polymer chains bridge neighboring particles through loops and tails. Furthermore, differences in milling methods likely modified the particle surface characteristics, including roughness, defect density, and adsorption site availability, resulting in different polymer adsorption behavior and floc structures despite comparable electrokinetic properties. Consequently, zeta potential alone is insufficient to predict settling performance, as floc size, density, and strength are the dominant factors governing sedimentation.

Overall, the combination of electrokinetic and settling results indicates that flocculation efficiency depends not only on zeta potential but also on the balance between surface charge neutralization and polymer bridging. The most effective clarification was achieved when the absolute zeta potential remained close to zero, providing sufficient destabilization to facilitate inter-particle collisions while maintaining adequate polymer bridging between adjacent particles. Excessive electrolyte concentration or polymer dosage shifted the surface charge beyond the optimal range, thereby reducing flocculation efficiency by promoting particle re-stabilization or suppressing bridging interactions. These findings are consistent with the classical DLVO framework and the widely reported polymer-bridging mechanism for mineral suspensions, confirming that electrokinetic measurements provide valuable insight into the mechanisms controlling coagulation and flocculation.

3.4. Energy barrier analysis

Interaction energies calculated using XDLVO theory provide a theoretical framework for interpreting the experimentally observed coagulation and flocculation behaviors. As shown in Fig. 11A, the interaction energy calculated per unit particle radius remained nearly constant for both electrolyte

systems; values of approximately 1.5 × 10^{19} KT μm^{-1} for the ball-mill product and 2.2 × 10^{18} KT μm^{-1} for the rod-mill product were obtained. The relatively small difference in interaction energy between NaCl and $CaCl_2$ indicates that both electrolytes significantly reduced the electrostatic energy barrier predicted by the XDLVO model. However, the settling rate increased slightly in the presence of $CaCl_2$ for both grinding products. While the settling rate of the ball-mill product increased from approximately 11.60 × 10^2 cm/sec to 11.66 × 10^2 cm/sec, a similar increase was observed for the rod-mill product. Although the difference was limited, this finding is consistent with the greater coagulating capability of Ca^{2+} ions, arising from their greater ability to compress the electrical double layer and promote specific ion adsorption. These observations are further supported by zeta potential measurements, which indicate a positive surface charge in the presence of $CaCl_2$.

The turbidity measurements also corroborated the XDLVO predictions. Although the calculated interaction energies were similar, the suspensions treated with $CaCl_2$ generally exhibited lower residual turbidity during settling compared to those treated with NaCl. This suggests that the improved clarification achieved with $CaCl_2$ stems not only from a reduction in electrostatic repulsion but also from specific chemical interactions, such as calcium bridging between negatively charged surface sites.

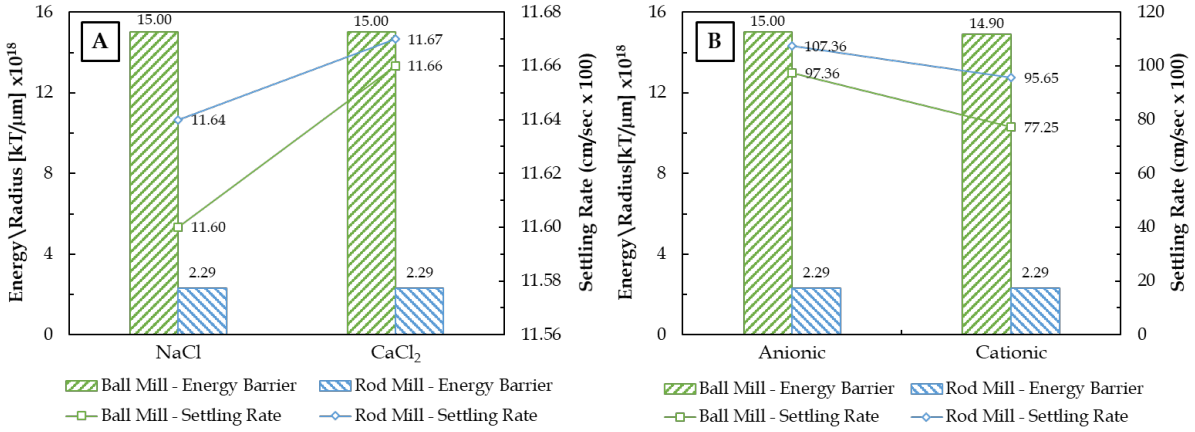

Fig. 11. Energy barrier heights calculated and corresponding settling rate values under constant (A) coagulant concentration (1×10^{-3} mol/dm^3) and (B) flocculant dosage (5 g/Mg)

Although total interaction energy cannot fully explain these interactions, it significantly influences aggregate density and settling characteristics. Consequently, the combination of XDLVO and experimental findings indicates that coagulation efficiency depends on both the magnitude of the interaction energy barrier and the nature of the adsorbed ions. Fig. 11B illustrates the effect of polymer type. The calculated interaction energy remained essentially unchanged after adding anionic or cationic flocculants, indicating that polymer addition after the particles had destabilized during coagulation did not substantially alter the total particle-particle interaction energy predicted by the XDLVO model. In contrast, the two polymer systems showed markedly different settling behavior. While the anionic flocculant yielded the highest settling rates for both grinding products, the cationic flocculant significantly decreased the settling rate.

While the value for the ball-mill product decreased from approximately 98 × 10^2 cm/sec to 77 × 10^2 cm/sec, the value for the rod-mill product decreased from approximately 106 × 10^2 cm/sec to 95 × 10^2 cm/sec. The higher settling rate with the anionic polymer is consistent with the zeta potential results, indicating that at 5 g/Mg the suspension remained near the electrokinetic instability region ($\zeta \approx -4.7$ mV). Under these conditions, electrostatic repulsion is sufficiently suppressed to enable extensive polymer bridging between adjacent particles, resulting in large, compact flocs with high settling velocities. In contrast, although the cationic polymer also yields a low absolute zeta potential value, its adsorption mechanism involves stronger electrostatic binding to the negatively charged mineral surfaces, resulting in a flatter polymer conformation with fewer loops and tails extending into solution. This adsorption configuration reduces the number of effective bridging sites available for interparticle bonding, thereby resulting in smaller or less permeable flocs that settle more slowly. Consequently, the

observed differences in settling performance arise primarily from the polymer adsorption configuration rather than from changes in the calculated interaction energy.

The turbidity measurements (Figs. 7 and 8) further support this interpretation. The systems with the highest settling rates consistently exhibited the greatest reduction in turbidity over settling time, whereas suspensions with lower settling velocities retained higher residual turbidity. These observations demonstrate that clarification efficiency is closely associated not only with particle destabilization but also with the formation of larger and denser flocs. Although XDLVO theory successfully predicts the reduction in the interaction energy barrier required for coagulation, it does not explicitly account for polymer-chain architecture, bridging efficiency, or floc morphology. Consequently, similar energy values can yield different separation performance depending on polymer properties and adsorption behavior.

The literature reports similar dependencies for ultrafine chromite and kaolinite suspensions (Panda et al., 2014). The selective flocculation studies showed that the highest recoveries and lowest turbidity values were obtained when sufficient polymer adsorption promoted selective bridge formation between valuable mineral particles while maintaining adequate dispersion of gangue minerals. Likewise, two-stage polymer dosing strategies for kaolinite tailings have been shown to reduce residual turbidity more effectively than single-stage addition because sequential adsorption promotes more uniform bridge formation and stronger aggregates. Dwari et al. (2018) investigated the flocculation of chromite beneficiation tailings using polyacrylamide flocculants. They reported that both low-ionicity anionic and highly cationic polymers produced excellent clarification efficiencies, achieving settling rates of approximately 19.5 cm/min together with very low supernatant turbidity at an optimum dosage of 15 g/Mg. Their results demonstrated that turbidity removal depended strongly on polymer molecular structure and adsorption configuration rather than solely on electrostatic charge neutralization. In another study on the possible effect of an energy barrier between particle-particle interactions, it was reported that as the calculated energy barrier decreases, attachment efficiency increases, resulting in faster aggregate growth and lower residual turbidity. Nevertheless, once polymer overdosing occurs, the interaction energy profile may remain favorable for collision while steric stabilization limits irreversible attachment. Consequently, turbidity increases despite a relatively low electrostatic energy barrier. This phenomenon explains why systems exhibiting charge reversal or near-zero zeta potential do not necessarily achieve maximum clarification efficiency (Zeng et al. 2026).

Overall, XDLVO calculations, zeta potential measurements, settling-rate analyses, and turbidity data indicate that coagulation and flocculation proceed via complementary mechanisms. While coagulation is primarily governed by reducing electrostatic interaction energy through electrical double-layer compression and charge neutralization, flocculation is mainly driven by polymer bridging once the energy barrier has been sufficiently lowered. Consequently, optimum separation performance was achieved when the interaction energy barrier predicted by the XDLVO model was low, the absolute zeta potential remained close to zero, and the polymer adopted an adsorption configuration capable of forming extensive interparticle bridges. The strong agreement between theoretical predictions and experimental observations confirms that the XDLVO approach provides a robust mechanistic framework for interpreting coagulation-flocculation behavior in mineral suspensions and highlights the importance of incorporating polymer adsorption when evaluating flocculation performance.

4. Conclusions

In this study, the coagulation and flocculation behavior of chromite mineral suspension was successfully evaluated by combining electrokinetic measurements, XDLVO interaction energy calculations, settling experiments, and turbidity analyses. The results demonstrated that both the electrolyte type and polymer properties significantly influenced particle aggregation and subsequent solid-liquid separation.

The zeta potential measurements demonstrated that the addition of NaCl and $CaCl_2$ effectively destabilized the suspension by reducing electrostatic repulsion; $CaCl_2$ exhibited a stronger coagulating effect due to the higher valence of Ca^{2+} ions, which compressed the electrical double layer and promoted specific ion adsorption. The XDLVO calculations revealed relatively low interaction energy barriers un-

der both electrolyte conditions and confirmed that the particle surfaces were thermodynamically favorable for aggregation. Although the calculated interaction energies were similar for NaCl and $CaCl_2$, the slightly higher settling rates and lower residual turbidity observed with $CaCl_2$ suggest that calcium-mediated interactions contributed to the formation of stronger, denser aggregates.

The flocculation results further demonstrated that polymer dosage and ionic character determine particle aggregation efficiency. At the investigated dosage, the anionic flocculant yielded higher settling rates and lower turbidity than the cationic flocculant, indicating more effective polymer bridging and floc formation. The zeta potential data also revealed that excessive polymer adsorption altered the particle surface charge, indicating the onset of surface overcharging and partial re-stabilization, which is consistent with the reduced clarification observed at higher reagent dosages.

Overall, the theoretical predictions from the XDLVO model showed good agreement with the experimental settling and turbidity measurements, demonstrating that reducing the interaction energy barrier is a prerequisite for efficient coagulation. However, the results also indicate that optimal flocculation cannot be explained solely by interaction energy; it also depends significantly on polymer adsorption behavior and bridging efficiency. Consequently, combining XDLVO analysis, zeta potential measurements, and experimental settling tests provides a comprehensive and reliable methodology for understanding and optimizing coagulation-flocculation processes in mineral processing.

Acknowledgments

This study is supported by the Scientific and Technological Research Council of Turkey (TUBITAK) with Project Number 124M905.

A part of the results reported in this paper was presented at XX Balkan Mineral Processing Congress BMPC2026 entitled "The contribution of roughness parameter on coagulation and flocculation characteristics of fine chromite".

References

AMUDA, O.S., AMOO, I.A., 2007. *Coagulation/flocculation process and sludge conditioning in beverage industrial wastewater treatment.* Journal of Hazardous Materials, 141, 3, 778-783.

CELİK, M.S., GUVEN, O., KARAAĞAÇLIOĞLU, İ.E., OZDEMİR, O., 2024. *Does hemimicelle concentration (HMC) coincide with critical aggregation concentration (CAC) in flotation.* Minerals Engineering, 215, 108812.

DRELICH, J.W., BOWEN, P., 2016. *Hydrophobic nano-asperities in control of energy barrier during particle–surface interactions*. Surface Innovations, 3,3, 164-171.

DWARI, R.K., ANGADI, S.I., TRIPATHY, S.K., 2018. *Studies on flocculation characteristics of chromite's ore process tailing: Effect of flocculants ionicity and molecular mass*. Colloids and Surfaces A: Physicochemical and Engineering Aspects, 537, 467-477.

ERSOY, B., 2005. *Effect of pH and polymer charge density on settling rate and turbidity of natural stone suspensions.* International Journal of Mineral Processing, 75, 207-216.

GUNGOREN, C., GUVEN, O., CINAR, M., OZDEMIR, O., 2020. *An investigation of the effect of clay type on coal flotation along with DLVO theoretical analyses*. International Journal of Coal Preparation and Utilization, 40, 3, 210-222.

GUVEN, O., OZDEMIR, O., KARAAGACLIOGLU, E., CELIK M.S., 2015. *Surface morphologies and floatability of sandblasted quartz particles*. Minerals Engineering, 70, 1–7.

GUVEN, O., CELIK, M.S., 2016. *Interplay of particle shape and surface roughness to reach maximum flotation efficiencies depending on collector concentration*. Mineral Processing and Extractive Metallurgy Review, 37,6, 412-417.

GUVEN, O., SERDENGEÇTI, M.T., TUNÇ, B., ÖZDEMIR, O., KARAAĞAÇLIOĞLU, İ.E., ÇELIK, M.S., 2020. *Effect of particle shape properties on selective separation of chromite from serpentine by flotation*. Physicochemical Problems of Mineral Processing, 56,5, 818-828.

GUVEN, O., KAYMAKOĞLU, B., EHSANI, A., HASSANZADEH, A., SIVRIKAYA, O., 2022. *Effects of grinding time on morphology and collectorless flotation of coal particles*. Powder Technology, 399, 117010.

GUVEN, O., KAYABAŞI, H.R., EHSANI, A., KAYMAKOĞLU, B., KARA, T.D.T., 2025. *The effect of grinding type on roughness and coagulation of magnesite particles*. Physicochemical Problems of Mineral Processing, 61,3, 203708

GUVEN, O., KAYABAŞI, H., DADAY, M., BIRINCI, M., OZDEMIR, O., 2026. *Effect of chloride salts on coagulation behaviour of* chromite *particles having different roughness produced by rod and ball mills*. Canadian Metallurgical Quarterly, 1-10.

MEGERSA, M., GACH, W., BEYENE, A., AMBELU, A., TRIEST, L., 2019. *Effect of salt solutions on coagulation performance of Moringa stenopetala and Maeruasubcordata for turbid water treatment*. Separation and Purification Technology, 221, 319-324.

MEI, L., GUAN, G., 2023. *Profilometry and atomic force microscopy for surface characterization*. Nano Transmed, 2, 1, e9130017.

MUHLE, K., 1985. *Particle adhesion in coagulation and bridging flocculation*. Colloid & Polymer Sci, 263, 660–672.

OZKAN, A., 2003. *Coagulation and flocculation characteristics of talc by different flocculants in the presence of cations*. Minerals Engineering, 16,1, 59-61.

OZUN, S., ULUS, D.A., 2019. *Coagulation and flocculation behavior of fines in foid-bearing rock processing plant (FRPP) wastewater at alkaline environment*. Powder Technology, 344, 335-342.

ÖNEN, V., GÖÇER, M., TANER, H.A., 2018. *Effect of coagulants and flocculants on dewatering of kaolin suspensions*. Omer Halisdemir University Journal of Engineering Sciences, 7, 1, 297-305.

PANDA, L., BANERJEE, P.K., BİSWAL, S.K., VENUGOPAL, R., MANDE, N.R., 2014. *Modelling and optimization of process parameters for beneficiation of ultrafine chromite particles by selective flocculation*. Separation and Purification Technology, 132, 666-673.

SHULEPOV, S. YU, FRENS, G., 1996. *Surface roughness and particle size effect on the rate of perikinetic coagulation: experimental*. Journal of Colloid and Interface Science, 182,388–394.

SURESH, L. AND WALZ, J.Y., 1996. *Effect of surface roughness on the interaction energy between a colloidal sphere and a flat plate*, Journal of Colloid and Interface Science, 183, 199–213.

TAYEBİ, N., POLYCARPOU, A., 2004. *Modeling the effect of skewness and kurtosis on the static friction coefficient of rough surfaces*. Tribology International, 37,6, 491-505

ULUSOY, U., 2023. *A review of particle shape effects on material properties for various engineering applications: From macro to nanoscale*. Minerals, 13,1, 91.

ULUSOY, U., YEKELER, M., HIÇYILMAZ, C., 2003. *Determination of the shape, morphological and wettability properties of quartz and their correlations*. Minerals Engineering, 16, 10, 951–964.

VERRELLI, D.I., BRUCKARD, W.J., KOH, P.T.L., 2014. *Particle shape effects in flotation. Part 1: Microscale experimental observations*. Minerals Engineering, 58, 80–89.

YEKELER, M., ULUSOY, U., HIÇYILMAZ, C., 2004. *Effect of particle shape and roughness of talc mineral ground by different mills on the wettability and floatability*. Powder Technology. 140, 1–2, 68–78.

ZENG, H., PENG, M., YU, J., ZHANG, L., LIU, J., HE, H., WANG, Z., 2026. *Forecasting flocculation process through collision-XDLVO theory*. Separation and Purification Technology, 387, 136723.

ZHANG, Z., WAN, L., MENG, X., XIE, Y., TIAN, H., MAO, D., DONG, W., SUN, X., MA, X., HUANG, Y., 2024. *Robotic wire-based friction stir additive manufacturing*. Additive Manufacturing, 88, 104261.

ZHANG, Z., WAN, L., WEN, Q., SHI, Y., FENG, Z., 2025. *Wire-based friction stir additive manufacturing of TiC reinforced Al-Cu-Mg composite: Particle refinement and dispersion*. Composites Part A: Applied Science and Manufacturing, 196, 109009.